DOI: 10.1021/ic100843k

Inorganic Chemistry
Article

Single-Chain Magnets Constructed by Using the Strict Orthogonality of Easy-Planes: Use of Structural Flexibility to Control the Magnetic Properties

Takashi Kajiwara,*,†,‡ Hiroki Tanaka,† Motohiro Nakano,*,§ Shinya Takaishi,† Yasuhiro Nakazawa,∥ and Masahiro Yamashita†

†*Department of Chemistry, Graduate School of Science, Tohoku University and CREST, Japan Science and Technology Agency (JST), Aramaki, Aoba-ku, Sendai 980-8578, Japan,* ‡*Department of Chemistry, Faculty of Science, Nara Women's University, Nara 630-8506, Japan,* §*Department of Applied Chemistry, Graduate School of Engineering, Osaka University, Suita, Osaka 565-0871, Japan, and* ∥*Department of Chemistry, Graduate School of Science, Osaka University, Toyonaka, Osaka 560-0043, Japan*

Received April 28, 2010

A family of single-chain magnets (SCMs), of which the SCM character originated from the spatial arrangement of high spin Fe^{II} ions with easy-plane anisotropy, was synthesized, and their magnetic properties were investigated. The chain complexes including alternating high-spin Fe^{II} ions and low-spin Fe^{III} ions, *catena*-$[Fe^{II}(ClO_4)_2\{Fe^{III}(bpca)_2\}]$-$ClO_4\cdot 3MeNO_2$ (**1**$\cdot 3MeNO_2$), *catena*-$[Fe^{II}(ClO_4)(H_2O)\{Fe^{III}(^{Me}\mathbf{L})_2\}](ClO_4)_2\cdot 2MeNO_2\cdot H_2O$ (**2**$\cdot 2MeNO_2\cdot H_2O$), *catena*-$[Fe^{II}(ClO_4)(H_2O)\{Fe^{III}(^{Bu}\mathbf{L})_2\}](ClO_4)_2\cdot 3.5MeNO_2$ (**3**$\cdot 3.5MeNO_2$), and *catena*-$[\{Fe^{II}(ClO_4)(H_2O)Fe^{II}(H_2O)_2\}_{0.5}$-$\{Fe^{III}(^{Ph}\mathbf{L})_2\}](ClO_4)_{2.5}\cdot 4EtNO_2$ (**4**$\cdot 4EtNO_2$), were synthesized with the use of bridging ligand Hbpca (bis-(2-pyridylcarbonyl)amine)) and its derivatives of $H^{Me}\mathbf{L}$, $H^{Bu}\mathbf{L}$, and $H^{Ph}\mathbf{L}$ each incorporating methyl, *tert*-butyl, or phenyl group on the 4-position of pyridyl ring. These complexes showed a typical ferrimagnetic behavior on direct current (dc) susceptibility data, and from an alternating current (ac) susceptibility measurements, SCM or superparamagnetic behaviors were confirmed with the Δ/k_B values of 22.5(4), 21.8(18), and 28.8(3) K for **1**$\cdot 3MeNO_2$, **2**$\cdot 2MeNO_2\cdot H_2O$, and **3**$\cdot 3.5MeNO_2$, of which the easy-axis anisotropy was originated from the orthogonal arrangement of easy-planes of Fe^{II} ions. In the crystal structures, cylindrical voids were formed along the chain axis being surrounded by four chains in **1**$\cdot 3MeNO_2$, **2**$\cdot 2MeNO_2\cdot H_2O$, and **4**$\cdot 4EtNO_2$ and two chains in **3**$\cdot 3.5MeNO_2$, and solvent molecules as well as coordination-free perchlorate anions occupied these voids in a slightly different fashion depending on the complexes. **2**$\cdot 2MeNO_2\cdot H_2O$ maintains its chemical composition in a dried condition, whereas **1**$\cdot 3MeNO_2$, **3**$\cdot 3.5MeNO_2$, and **4**$\cdot 4EtNO_2$ easily release solvent molecules to give **1**, **3**, and **4**, respectively. **1** and **3** maintain the crystalline character showing slightly different X-ray diffraction (XRD) patterns from those of **1**$\cdot 3MeNO_2$ and **3**$\cdot 3.5MeNO_2$, and an enhancement of SCM character after release of the solvent molecules was observed for both. **4** lost crystalline character to become amorphous, and it lost the SCM character at the same time.

Introduction

One of the most fascinating developments in the past decade in the field of molecular-based magnetism is one-dimensional magnetic chains. One-dimensional magnetic chains that exhibit slow relaxation of the magnetization, known as superparamagnetic behavior, are called single-chain magnets (SCMs). SCMs are very hot topics in chemistry and material physics[1] because of their fundamental physical properties,[2,3] such as finite-sized effects. Such SCMs have been strategically constructed by linearly arranging the spin carrier components having an easy-axis type magnetic anisotropy ($D < 0$) to form Ising-type one-dimensional chains and a "double-well potential" which prevents the reversal of the molecular magnetic momentum. The following are a few examples: Co^{II}/nytronyl nytroxide radical,[4] Mn^{III}/Ni^{II},[5]

*To whom correspondence should be addressed. E-mail: kajiwara@cc.nara-wu.ac.jp (T.K.), moto@ch.wani.osaka-u.ac.jp (M.N.).

(1) Bogani, L.; Vindigni, A.; Sessoli, R.; Gatteschi, D. *J. Mater. Chem.* **2008**, *18*, 4750.

(2) (a) Coulon, C.; Clérac, R.; Lecren, L.; Wernsdorfer, W.; Miyasaka, H. *Phys. Rev. B* **2004**, 132408. (b) Vindigni, A. *Inorg. Chim. Acta* **2008**, *361*, 3731. (c) Coulon, C.; Clérac, R.; Lecren, L.; Wernsdorfer, W.; Miyasaka, H. *Phys. Rev. B* **2004**, *69*, 132408. (d) Luscombe, J. H.; Luban, M.; Reynolds, J. P. *Phys. Rev. E* **1996**, *53*, 5852. (e) Bogani, L.; Caneschi, A.; Fedi, M.; Gatteschi, D.; Massi, M.; Novak, M. A.; Pini, M. G.; Rettori, A.; Sessoli, R.; Vindigni, A. *Phys. Rev. Lett.* **2004**, *92*, 207204.

(3) (a) Sessoli, R. *Angew. Chem., Int. Ed.* **2008**, *47*, 5508. (b) Ishii, N.; Okamura, Y.; Chiba, S.; Nogami, T.; Ishida, T. *J. Am. Chem. Soc.* **2008**, *130*, 24.

(4) Caneschi, A.; Gatteschi, D.; Lalioti, N.; Sangregorio, C.; Sessoli, R.; Venturi, G.; Vindigni, A.; Rettori, A.; Pini, M. G.; Novak, M. A. *Angew. Chem., Int. Ed.* **2001**, *40*, 1760.

(5) (a) Clérac, R.; Miyasaka, H.; Yamashita, M.; Coulon, C. *J. Am. Chem. Soc.* **2002**, *124*, 12837. (b) Ferbinteanu, M.; Miyasaka, H.; Wernsdorfer, W.; Nakata, K.; Sugiura, K.-i.; Yamashita, M.; Coulon, C.; Clérac, R. *J. Am. Chem. Soc.* **2005**, *127*, 3090.

Published on Web 08/19/2010

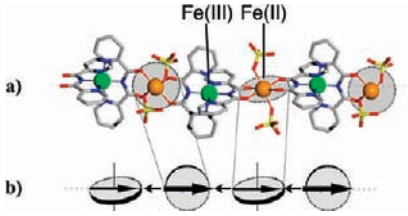

Figure 1. (a) Crystal structure and (b) spin arrangement of the cationic part of *catena*-$[Fe^{II}(ClO_4)_2\{Fe^{III}(bpca)_2\}]ClO_4\cdot 3MeNO_2$ ($\mathbf{1}\cdot 3MeNO_2$). Gray circles in (a) correspond to the equatorial planes (or easy-planes) of high spin Fe^{II} ions. Fe^{II} ions, orange; Fe^{III} ions, green; Cl, yellow; O, red; N, blue; C, gray.

Co^{II}/Fe^{III},[6] lanthanide (e.g., Dy^{III})/nytronyl nytroxide radical[7] chains, and so on.[8] We have reported a novel SCM constructed by using a twisted arrangement of spin carrier components with easy-plane type magnetic anisotropy (namely, hard-axis or XY plane anisotropy with $D > 0$), which generally helps avoiding bistability that leads to a "double-well potential".[9] The mixed-valence[10] chain complex *catena*-$[Fe^{II}(ClO_4)_2\{Fe^{III}(bpca)_2\}]ClO_4\cdot 3MeNO_2$ ($\mathbf{1}\cdot 3MeNO_2$, here Hbpca denotes bis-(2-pyridylcarbonyl)amine)), shown in Figure 1, is constructed with an alternating arrangement of high-spin Fe^{II} ions and low-spin Fe^{III} ions along the chains axis,[9] and Fe^{II} ($S = 2$) and Fe^{III} ($S = 1/2$) ions are connected in a ferrimagnetic manner. In $\mathbf{1}\cdot 3MeNO_2$, $bpca^-$ coordinates to the Fe^{III} ion in a *mer*-manner, and the equatorial planes of Fe^{II} ion, which correspond to easy-plane magnetic anisotropy, are in a twisted arrangement along the chain as a result. Consequently, the anisotropic planes (equatorial planes) of the Fe^{II} ions were arranged in a slightly tilted orthogonal manner along the chain. Each easy-plane has an easy-axis component along the chain, and an additive effect of these components results in the formation of an easy-axis anisotropy throughout the entire chain, thus giving $\mathbf{1}\cdot 3MeNO_2$ SCM character. The alternating current (ac) susceptibilities of $\mathbf{1}\cdot 3MeNO_2$ showed strong dependency on the frequency, which is typical for the SCM. The temperature dependency of their peak tops obeyed the Arrhénius law, and the activation energy barrier, Δ/k_B, was estimated to be 22.5(4) K. Moreover, the SCM behavior of $\mathbf{1}\cdot 3MeNO_2$ was affected by the absorption/desorption of the crystalline solvent molecules,[11] which is known as magnetic sponge-like behavior.[12] $\mathbf{1}\cdot 3MeNO_2$ can reversibly release or absorb nitromethane ($MeNO_2$) molecules, which causes a drastic change in magnetic properties.[11] Because of the uniaxial anisotropy of $\mathbf{1}\cdot 3MeNO_2$ that originates from the strict arrangement of the easy-plane of Fe^{II} ions and the magnetic interaction between Fe(II)−Fe(III) ions, the magnetic properties of this system might be very sensitive to the subtle change in the chain structure. In the other words, the magnetic properties of this system respond to changes in the chain structure. Thus, this twisted arrangement of easy-plane anisotropy shows that the magnetic properties can be controlled by the design of the molecular structure and the chain arrangement.

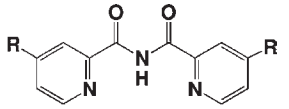

Figure 2. Structure of bis(4-*R*-2-pyridylcarbonyl)amine, where *R* denotes hydrogen, methyl, *tert*-butyl, or phenyl group.

In this paper, we report a correlation between subtle changes in the structure and the magnetic properties and details of solvent induced changes in the magnetic properties of a family of twisted XY chain complexes derived from $\mathbf{1}\cdot 3MeNO_2$, including *catena*-$[Fe^{II}(ClO_4)(H_2O)\{Fe^{III}(^{Me}\mathbf{L})_2\}](ClO_4)_2\cdot 2MeNO_2\cdot H_2O$ ($\mathbf{2}\cdot 2MeNO_2\cdot H_2O$, $^{Me}\mathbf{L}^-$ denotes bis-(4-methyl-2-pyridylcarbonyl)aminate),[13] *catena*-$[Fe^{II}(ClO_4)(H_2O)\{Fe^{III}(^{Bu}\mathbf{L})_2\}](ClO_4)_2\cdot 3.5MeNO_2$ ($\mathbf{3}\cdot 3.5MeNO_2$, $^{Bu}\mathbf{L}^-$ = bis(4-*tert*-butyl-2-pyridylcarbonyl)aminate) and *catena*-$[\{Fe^{II}(ClO_4)(H_2O)Fe^{II}(H_2O)_2\}_{0.5}\{Fe^{III}(^{Ph}\mathbf{L})_2\}](ClO_4)_{2.5}\cdot 4EtNO_2$ ($\mathbf{4}\cdot 4EtNO_2$, $^{Ph}\mathbf{L}^-$ = bis(4-phenyl-2-pyridylcarbonyl)aminate). To induce the structural changes in $\mathbf{1}\cdot 3MeNO_2$ keeping its SCM character, we introduced various substituent groups onto the $bpca^-$ ligand at the 4-position, as shown in Figure 2. The alternating arrangement of Fe^{II} and Fe^{III} ions as well as the twisted arrangement of easy planes of the Fe^{II} ions was retained in the resultant complexes; however, the positional relationship among the neighboring chains changed, leading to changes in the configuration of the pores that include solvent molecules. In addition, the steric repulsion among the bulky substituent groups caused structural perturbations in the chain complexes themselves. These two factors strongly affect both the SCM and the magnetic sponge characters.

Experimental Section

General Procedures and Materials. All chemicals and reagents were purchased as reagent grade and used without further purification. Solvents for syntheses were degassed with nitrogen. All chemical reactions and sample preparations for the measurement were carried out under an inert atmosphere.

Synthesis of 1,3,5-Tris(4-methyl-2-pyridyl)triazine (5).[14] 4-Methyl-2-cyanopyridine was obtained by reacting 4-methylpridine

(6) (a) Lescouëzec, R.; Vaissermann, J.; Ruiz-Pérez, C.; Lloret, F.; Carrasco, R.; Julve, M.; Verdaguer, M.; Dromzee, Y.; Gatteschi, D.; Wernsdorfer, W. *Angew. Chem., Int. Ed.* **2003**, *42*, 1483. (b) Toma, L. M.; Lescouëzec, R.; Pasán; Ruiz-Pérez, C.; Vaissermann, J.; Cano, J.; Carrasco, R.; Wernsdorfer, W.; Lloret, F.; Julve, M. *J. Am. Chem. Soc.* **2006**, *128*, 4842.

(7) (a) Bernot, K.; Bogani, L.; Caneschi, A.; Gatteschi, D.; Sessoli, R. *J. Am. Chem. Soc.* **2006**, *128*, 7947. (b) Bogani, L.; Sangregorio, C.; Sessoli, R.; Gatteschi, D. *Angew. Chem., Int. Ed.* **2005**, *44*, 5817.

(8) (a) Pardo, E.; Ruiz-García, R.; Lloret, F.; Faus, J.; Julve, M.; Journaux, Y.; Delgado, F.; Ruiz-Pérez, C. *Adv. Mater.* **2004**, 1597. (b) Toma, L. M.; Lescouëzec, R.; Lloret, F.; Julve, M.; Vaissermann, J.; Verdaguer, M. *Chem. Commun.* **2003**, 1850. (c) Miyasaka, H.; Madanbashi, T.; Sugimoto, K.; Nakazawa, Y.; Wernsdorfer, W.; Sugiura, K.-i.; Yamashita, M.; Coulon, C.; Clérac, R. *Chem.—Eur. J.* **2006**, *12*, 7028. (d) Lescouëzec, R.; Toma, L. M.; Vaissermann, J.; Verdaguer, M.; Delgado, F. S.; Ruiz-Pérez, C.; Lloret, F.; Julve, M. *Coord. Chem. Rev.* **2005**, *249*, 2691. (e) Chakov, N. E.; Wernsdorfer, W.; Abboud, K. A.; Christou, G. *Inorg. Chem.* **2004**, *43*, 5919. (f) Bai, Y.-L.; Tao, J.; Wernsdorfer, W.; Sato, O.; Huang, R.-B.; Zheng, L.-S. *J. Am. Chem. Soc.* **2006**, *128*, 16428.

(9) (a) Kajiwara, T.; Nakano, M.; Kaneko, Y.; Takaishi, S.; Ito, T.; Yamashita, M.; Igashira-Kamiyama, A.; Nojiri, H.; Ono, Y.; Kojima, N. *J. Am. Chem. Soc.* **2005**, *127*, 10150. (b) Kajiwara, T.; Watanabe, I.; Kaneko, Y.; Takaishi, S.; Enomoto, M.; Kojima, N.; Yamashita, M. *J. Am. Chem. Soc.* **2007**, *129*, 12360.

(10) Day, P.; Hush, N. S.; Clark, R. J. H. *Phil. Trans. Roy. Soc. A* **2007**, *366*, 5.

(11) Kaneko, Y.; Kajiwara, T.; Yamane, H.; Yamashita, M. *Polyhedron* **2007**, *26*, 2074.

(12) (a) Kahn, O.; Larionova, J.; Yakhmi, J. V. *Chem.—Eur. J.* **1999**, *5*, 3443. (b) Maspoch, D.; Ruiz-Molina, D.; Wurst, K.; Domingo, N.; Cavallini, M.; Biscarini, F.; Tejada, J.; Rovira, C.; Veciana, J. *Nat. Mater.* **2003**, *2*, 190. (c) Ohkoshi, S.-i.; Arai, K.-i.; Sato, Y.; Hashimoto, K. *Nat. Mater.* **2004**, *3*, 857.

(13) Tanaka, H.; Kajiwara, T.; Kaneko, Y.; Takaishi, S.; Yamashita, M. *Polyhedron* **2007**, *26*, 2105.

(14) (a) Case, F. H.; Koft, E. *J. Am. Chem. Soc.* **1959**, *81*, 905. (b) Chan, G. Y. S.; Drew, M. G. B.; Hudson, M. J.; Isaacs, N. S.; Byers, P. *Polyhedron* **1996**, *15*, 3385.

N-oxide and trimethylsilylcyanide according to the reported procedure.[15] This cyanopyridine (3.0 g, 25 mmol) was heated at 125 °C for 24 h in the presence of a catalytic amount of sodium hydride (60% dispersion in mineral oil, 0.1 g) to afford 1,3,5-tris(4-methyl-2-pyridyl)triazine. The crude product was dissolved in 100 mL of dichloromethane, and then 70 mL of *n*-heptane was added. The black precipitate was removed by filtration, and the resulting yellow solution was slowly concentrated to about 1/3 of the volume in air. The triazine was obtained as yellow crystalline compound (2.14 g, yield =71%).

^{1}H NMR ($CDCl_3$): δ = 8.81 (1H, d, J = 4.8 Hz), 8.68 (1H, s), 7.35 (1H, d, J = 4.9 Hz), 2.54 (3H, s) ppm.

1,3,5-Tris(4-*tert*-butyl-2-pyridyl)triazine (6)[14]**.** 4-*tert*-Butyl-2-cyanopyridine was obtained using the same procedure to prepare **5** with 4-*tert*-butylpridine *N*-oxide as the starting material.[15] The mixture of 4-*tert*-butylcyanopyridine (4.0 g, 25 mmol) and NaH (0.12 g, obtained from the 60% sodium hydride dispersed in mineral oil by washing with *n*-hexane) was heated at 125 °C for 24 h to give a black solid. The crude product was purified by column chromatography on alumina with chloroform as the eluent. The triazine was obtained as pale yellow crystals. Yield 1.59 g (40%).

^{1}H NMR ($CDCl_3$): δ = 8.47 (1H, d, J = 5.1 Hz), 8.23 (1H, d, J = 1.9 Hz), 7.43 (1H, dd, J = 5.2, 2.0 Hz), 1.35 (9H, s) ppm.

1,3,5-Tris(4-phenyl-2-pyridyl)triazine (7)[14,15]**.** 4-Phenyl-2-cyanopydine was obtained using the same procedure to prepare **5** with 4-phenylpridine *N*-oxide as the starting material. The cyanopyridine (3.3 g, 18 mmol) was heated at 125 °C for 24 h in the presence of a catalytic amount of sodium hydride (60% dispersion in mineral oil, 0.17 g) to afford 1,3,5-tris(4-phenyl-2-pyridyl)triazine. The crude product was first purified by column chromatography on alumina with chloroform as the eluent, and from the main fraction, a brown oily product was obtained. This oily product was dissolved in 50 mL of dichloromethane, and then 150 mL of *n*-heptane was added. The black precipitate was collected by filtration and was again purified by column chromatography on alumina using chloroform as the eluent. The triazine was obtained as a yellow solid. Yield 2.17 g (66%).

^{1}H NMR ($CDCl_3$): δ = 9.05 (1H, d, J = 1.7 Hz), 9.00 (1H, dd, J = 5.1, 0.9 Hz), 7.81 (2H, dd, J = 6.8, 9.8 Hz), 7.76 (1H, d, J = 5.1, 1.7 Hz), 7.57−7.54 (2H, br m), 7.51−7.49 (1H, br m) ppm.

Bis(4-methyl-2-pyridylcarbonyl)amine (8, $H^{Me}L$). An ethanolic solution (50 mL) of **5** (1.77 g, 5 mmol) and an aqueous solution (60 mL) of copper(II) nitrate (1.21 g, 5 mmol) were mixed, and the resulting deep brown solution was refluxed for 4 h. The resulting green solution was slowly evaporated to about 1/10 volume in the air, and blue plate crystals were obtained in a yield of 0.95 g, of which the composition was confirmed to be $[Cu^{II}(^{Me}L)(H_2O)_2]NO_3\cdot 3H_2O$ (**9**$\cdot 3H_2O$) by using X-ray analysis (see Supporting Information, Figure S1). IR (cm^{-1}): ν (CO) 1714 (s).

9$\cdot 3H_2O$ (0.95 g) and an excess of Na_2H_2edta (2.0 g, 5.4 mmol) were suspended in a H_2O (80 mL)/$CHCl_3$ (50 mL) mixture, and the suspension was vigorously stirred for 1 h. The resulting clear solution was separated, and the yellow organic layer was dried with sodium sulfate and evaporated under reduced pressure. **8** was obtained as yellow crystals with a yield of 0.28 g (22% based on **5**).

Elemental anal.; Found: C, 65.50; H, 5.40; N, 16.67. Calcd. for $C_{14}H_{13}N_3O_2$ ($H^{Me}L$): C, 65.87 ; H, 5.13; N, 16.46. IR (cm^{-1}): ν(CO) 1758 (s) ^{1}H NMR ($CDCl_3$): δ = 2.45 (s, 6H), 7.26 (d, 1H), 7.37 (d, 1H), 8.04 (s, 1H), 8.17 (s, 1H), 8.42 (d, 1H), 8.60 (d, 1H) ppm.

(15) (a) Shuman, R. T.; Ornstein, P. L.; Paschal, J. W.; Gesellchen, P. D. *J. Org. Chem.* **1990**, *55*, 738. (b) Bell, Z. R.; Motson, G. R.; Jeffery, J. C.; McCleverty, J. A.; Ward, M. D. *Polyhedron* **2001**, *20*, 2045. (c) Hoyle, W. C.; Benga, J. *Talanta* **1980**, *27*, 963.

Bis(4-*tert*-butyl-2-pyridylcarbonyl)amine (10, $H^{Bu}L$). An aqueous suspension (6 mL) of **6** (1.44 g, 3 mmol) and an aqueous solution (24 mL) of copper(II) sulfate (1.50 g, 6 mmol) were mixed, and the resulting deep green solution was refluxed for 4 h, during which the color changed to deep blue. This solution was cooled to room temperature, and a blue powder of $\{Cu^{II}(^{Ph}L)\}^+$ compound precipitated, which was collected by filtration and dried. This powder was used for the next reaction without further purification. Yield 0.90 g. IR (cm^{-1}): ν (CO) 1711 (s).

The blue powder (0.90 g) and excess Na_2H_2edta (2.0 g, 5.4 mmol) were suspended in a H_2O (80 mL)/$CHCl_3$ (50 mL) mixture, and the suspension was vigorously stirred for 1 h. The resulting clear solution was separated, and the pale green organic layer was dried with sodium sulfate and evaporated under reduced pressure. **10** was obtained as pale green crystals in a yield of 0.18 g (18% based on **6**).

Elemental analysis calcd for $C_{20}H_{25.67}N_3O_{2.33}$ (**10**$\cdot 1/3H_2O$): C 69.54, H 7.49, N 12.16; Found: C 69.39, H 7.27, N 12.31. IR (cm^{-1}): ν(CO) 1758 (s) ^{1}H NMR ($CDCl_3$): δ = 1.38 (s, 18H), 7.53 (d, 1H), 7.54 (d, 1H), 8.34 (d, 1H), 8.35 (d, 1H), 8.64 (d, 1H), 8.65 (d, 1H) ppm.

Bis(4-phenyl-2-pyridylcarbonyl)amine (11, $H^{Ph}L$). An ethanolic suspension (60 mL) of **7** (1.08 g, 2 mmol) and an aqueous solution (20 mL) of copper(II) perchlorate (2.22 g, 6 mmol) were mixed, and the resulting deep brown solution was refluxed for 4 h, during which the color changed to deep blue. The solution was cooled to room temperature, and the blue powder that precipitated was collected by filtration and dried. Yield 0.92 g. The composition of this compound was confirmed to be $[Cu^{II}(^{Ph}L)(H_2O)_2]ClO_4$ (**12**) by using X-ray analysis (see Supporting Information, Figure S2). This powder was used for the next reaction without further purification. IR (cm^{-1}): ν (CO) 1711 (s).

The blue powder (0.90 g) and excess Na_2H_2edta (2.0 g, 5.4 mmol) were suspended in a H_2O (80 mL)/$CHCl_3$ (50 mL) mixture, and the suspension was vigorously stirred for 7 days. The resulting clear solution was separated, and the pale green organic layer was dried over sodium sulfate and evaporated under reduced pressure to give pale green crystals of **11** in a yield of 0.15 g (19% based on **7**).

Elemental analysis (%) calcd for $C_{24}H_{19}N_3O_3$ (**11**$\cdot H_2O$): C 72.53, H 4.81, N 10.57; found: C 72.28, H 4.73, N 10.81. IR (cm^{-1}): ν(CO) 1758 (s) ^{1}H NMR ($CDCl_3$): δ = 7.51 (t, 3H), 7.76 (d, 2H), 7.78 (d, 1H), 8.60 (s, 1H), 8.81 (d, 1H) ppm.

Synthesis of $[Fe^{III}(^{Me}L)_2]ClO_4$ (12). To a solution of $H^{Me}L$ (351 mg, 1.37 mmol) in 20 mL of acetone was added an aqueous solution (10 mL) of iron(III) nitrate (284 mg, 0.81 mmol). To the mixture was added excess Et_4NClO_4 (987 mg, 4.3 mmol), and the resulting dark green solution was allowed to stand for 4−5 days to afford **12** as dark brown crystals. They were collected by suction filtration, washed with a minimum amount of acetone, and dried in vacuo. Yield 310 mg (66%)

Elemental analysis (%) calcd for $FeC_{28}H_{26}N_6O_9Cl$ (**12**$\cdot H_2O$): C 49.32, H 3.85, N 12.32; found: C 49.23, H 4.24, N 12.15. IR (cm^{-1}): ν(CO) 1758 (s); ν(ClO_4) 1095 (s).

Synthesis of $[Fe^{III}(^{Bu}L)_2]ClO_4$ (13). To a solution of $H^{Bu}L$ (500 mg, 1.4 mmol) in 70 mL of acetone was added an aqueous solution (20 mL) of iron(III) perchlorate (384 mg, 0.83 mmol). The brown suspension was stirred at room temperature for 5 h, and the resulting orange solution was allowed to stand for 1−2 days to afford **13** as orange crystals. They were collected by suction filtration, washed with a minimum amount of acetone, and dried in vacuo. Yield 350 mg (56%)

Elemental analysis (%) calcd for $FeC_{40}H_{54}N_6O_{11}Cl$ (**13**$\cdot 3H_2O$): C 54.21, H 6.14, N 9.48; found: C 54.27, H 6.02, N 9.61. IR (cm^{-1}): ν(CO) 1758 (s); ν(ClO_4) 1758 (s).

Synthesis of $[Fe^{III}(^{Ph}L)_2]ClO_4$ (14). To a solution of $H^{Ph}L$ (530 mg, 1.3 mmol) in 140 mL of acetone and 15 mL of methanol was added an aqueous solution (20 mL) of iron(III) perchlorate

(384 mg, 0.83 mmol). The obtained orange solution was allowed to stand for 1−2 days to yield **14** as orange crystals. They were collected by suction filtration, washed with a minimum amount of acetone, and dried in vacuo. Yield 220 mg (36%).

Elemental analysis (%) calcd for $FeC_{48}H_{34}N_6O_9Cl$ (**14**·H_2O): C 61.98, H 3. 68, N 9.04; found: C 61.60, H 3.97, N 8.99. IR (cm^{-1}): ν(CO) 1758 (s); $\nu(ClO_4)$ 1758 (s)

Preparation of *catena*-[$Fe^{II}(ClO_4)(H_2O)\{Fe^{III}(^{Me}L)_2\}](ClO_4)_2$·$2MeNO_2$·$H_2O$ (2·2$MeNO_2$·H_2O). To a nitromethane solution of **12**·H_2O (10 mM, 2 mL) was added a solution of $[Fe^{II}(H_2O)_6](ClO_4)_2$ (7.24 mg, 20 μmol) in one drop of water. The resulting solution was allowed to stand for 2 weeks, during which time black rod-like crystals of **2**·2$MeNO_2$·H_2O suitable for X-ray crystallography formed. They were collected by using filtration under a nitrogen atmosphere and washed with a minimum amount of nitromethane. Yield 1.0 mg, 4.7%.

Elemental analysis (%) calcd for $Fe_2C_{30}H_{34}N_8O_{22}Cl_3$ (**2**·2$MeNO_2$·H_2O): C 33.47, H, 3.18; N, 10.37; found: C 33.31, H 3.39, N 10.32.

Preparation of *catena*-[$Fe^{II}(ClO_4)(H_2O)\{Fe^{III}(^{Bu}L)_2\}](ClO_4)_2$·$3.5MeNO_2$ (3·3.5$MeNO_2$). Complex **3**·3.5$MeNO_2$ was synthesized similar to **2**·2$MeNO_2$ using **13**·3H_2O instead of **12**·H_2O. Black needle-like crystals of **3**·3.5$MeNO_2$ suitable for X-ray crystallography grew from the reaction mixture in 3−4 days. They were collected by using filtration under nitrogen and washed with a minimum amount of nitromethane. Yield 30.6%.

Elemental analysis (%) calcd for $Fe_2C_{43}H_{59}N_9O_{23}Cl_3$ (**3**·3.5$MeNO_2$): C 39.62, H 4.62, N 10.09; found: C 39.78, H 4.65, N 9.88.

Preparation of *catena*-[{$Fe^{II}(ClO_4)(H_2O)Fe^{II}(H_2O)_2\}_{0.5}\{Fe^{III}(^{Ph}L)_2\}](ClO_4)_{2.5}$·$4EtNO_2$ (4·4$EtNO_2$). To a nitroethane solution (2 mL) of **14**·H_2O (18.6 mg, 20 μmol) was added a solution of $[Fe^{II}(H_2O)_6](ClO_4)_2$ (7.24 mg, 20 μmol) in one drop of methanol. The resulting solution was allowed to stand for 1−2 days, during which time black needle-like crystals of **4**·4$EtNO_2$ suitable for X-ray crystallography formed. They were collected by using filtration under a nitrogen atmosphere and washed with a minimum amount of nitroethane. Yield 5.4 mg, 18.2%.

Elemental analysis (%) calcd for $Fe_2C_{56}H_{55}N_{10}O_{25.5}Cl_3$ (**4**·4$EtNO_2$): C 45.02, H 3.71, N 9.37; found: C 44.93, H 3.78, N 9.20.

Magnetic Measurements. Magnetic susceptibility measurements were performed on a Quantum Design SQUID magnetometer MPMS-5S. The solvated samples **1**·3$MeNO_2$, **2**·2$MeNO_2$·H_2O, **3**·3.5$MeNO_2$, and **4**·4$EtNO_2$ were encaged into closed capsules or covered with grease to avoid the removal of solvent molecules. Since the dried samples were hygroscopic, completely dried samples **1**, **3**, and **4** were prepared in a glovebox and attached quickly to the equipment to avoid the exposure to the air. The direct current (dc) measurements were performed in the temperature range of 2.0−300 K and in a field range from −50 to 50 kOe. The alternating current (ac) measurements were performed at various frequencies from 5 to 997 Hz with an ac field amplitude of 3 Oe and no dc field applied. Diamagnetic corrections for the samples were determined from Pascal's constants.

The investigation of dc susceptibility in the temperature range of 0.5−1.8 K was made on an iQUANTUM iHelium3 apparatus.

Crystal Structure Analyses. Single crystal X-ray data were collected at low temperature on a Bruker AXS SMART-APEX/CCD area detector using graphite monochromated Mo Kα radiation (0.71079 Å). The intensity data were empirically corrected for absorption with using the program SADABS.[16] The structures were solved by direct methods using SIR97,[16] and structure refinements were carried out using Full-matrix least-squares calculations (SHELXL-97).[16] Non-hydrogen atoms except for some solvent molecules and disordered molecules were refined anisotropically, and the hydrogen atoms were treated using a riding model.

X-ray powder diffraction patterns were collected on a Rigaku RINT 2500 powder diffractometer with Bragg−Brentano geometry using Cu Kα radiation (1.5418 Å).

Thermo-Gravimetry (TG) Measurements. TG measurements were carried out under a dry nitrogen atmosphere on a Shimadzu DTG-60H analyzer.

(16) *SHELXTL*, PC Package; Bruker, AXS Inc.: Madison, WI, 1998.

Results and Discussions

Structures. The structure for **1**·3$MeNO_2$, which has already been reported and discussed,[9] is presented together with the other chain complexes for the comparison. Crystal structures of the complexes are shown in Figures 3 and 4, and crystallographic data for all complexes are summarized in Table 1. Each of these complexes is composed of an alternate arrangement of Fe^{II} ions and $\{Fe^{III}(\mathbf{L})_2\}$ units ($\mathbf{L}$ = $bpca^-$ and its derivatives) to form mixed-valence infinite chains. The equatorial sites of the octahedral Fe^{II} ions are occupied by four carbonyl oxygen atoms from two $\{Fe^{III}(\mathbf{L})_2\}$ units, and the axial positions are occupied by water molecule(s) and/or perchlorate ion(s), depending on the complex.

Compound **2**·2$MeNO_2$·H_2O crystallized in the triclinic space group $P\bar{1}$ (Z = 4). The unit cell included two independent pairs of $\{Fe^{III}(^{Me}\mathbf{L})_2\}^+$ and $\{Fe^{II}(ClO_4)(H_2O)\}^+$ units with similar structures and two $MeNO_2$ molecules and a water molecule per each Fe^{II}/Fe^{III} pair as solvents of crystallization. The formula of complex **2** was determined to be $[Fe^{II}(ClO_4)(H_2O)\{Fe^{III}(^{Me}\mathbf{L})_2\}](ClO_4)_2$ which includes one water molecule and one perchlorate ion axially coordinated to the Fe^{II} ions. Selected bond distances for each complex are summarized in Table 2.

Complex **3**·3.5$MeNO_2$ crystallized in the monoclinic space group $P2_1/n$ (Z = 4). The structure contains an independent pair of $\{Fe^{III}(^{Bu}\mathbf{L})_2\}^+$ and $\{Fe^{II}(ClO_4)(H_2O)\}^+$ units and three and a half $MeNO_2$ as solvents of crystallization. The Fe^{II} ions in **3**·3.5$MeNO_2$ are coordinated by one water molecule and one perchlorate anion in axial positions similar to **2**·2$MeNO_2$·H_2O.

The structure of complex **4**·4$EtNO_2$ was more complicated compared to those of **2**·2$MeNO_2$·H_2O and **3**·3.5$MeNO_2$. **4**·4$EtNO_2$ crystallized in the monoclinic space group $P2_1/n$ (Z = 8). In the structure, there is a crystallographically independent array of $\{Fe^{III}(^{Ph}\mathbf{L})_2\}^+$, $\{Fe^{II}(ClO_4)(H_2O)\}^+$, $\{Fe^{III}(^{Ph}\mathbf{L})_2\}^+$, and $\{Fe^{II}(H_2O)_2\}^{2+}$ units arranged in an alternating manner to form infinite chains. The complex includes two different Fe^{II} ions in axial coordination patterns in which a water molecule and a perchlorate ion are coordinated to one and two water molecules to the other. Many solvent molecules were included in the cell showing heavy disordering, and exact analyses were hard to be carried out. From the elemental analysis as well as the thermo-gravimetric measurement, eight $EtNO_2$ molecules were found per each $Fe^{II}/Fe^{III}/Fe^{II}/Fe^{III}$ array giving the formula of *catena*-[{$Fe^{II}(ClO_4)(H_2O)\}\{Fe^{III}(^{Ph}\mathbf{L})_2\}\{Fe^{II}(H_2O)_2\}\{Fe^{III}(^{Ph}\mathbf{L})_2\}](ClO_4)_5$·$8EtNO_2$, which is written as *catena*-[{$Fe^{II}(ClO_4)_{0.5}(H_2O)_{1.5}\}\{Fe^{III}(^{Ph}\mathbf{L})_2\}](ClO_4)_{2.5}$·$4EtNO_2$ (**4**·4$EtNO_2$) hereafter.

In all complexes, each high-spin Fe^{II} ion in the $\{Fe^{II}(ClO_4)(H_2O)\}^+$ or $\{Fe^{II}(H_2O)_2\}^{2+}$ unit has an elongated

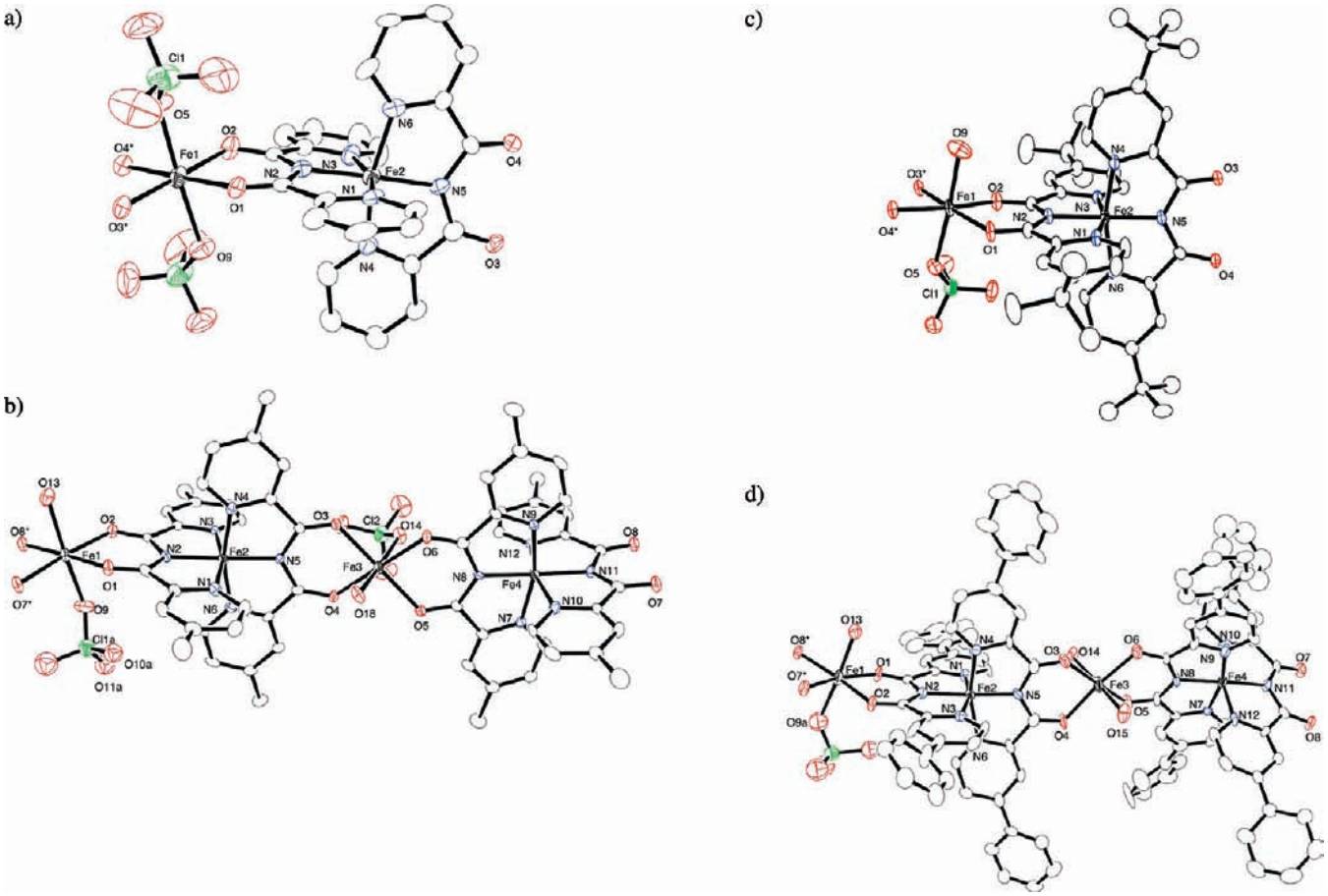

Figure 3. ORTEP drawings of the cationic parts of (a) **1**·3MeNO$_2$ with symmetry operation (*): $-0.5+x$, $0.5-y$, $0.5+z$, (b) **2**·2MeNO$_2$·H$_2$O with the symmetry operation (*): $+x$, $-1+y$, $-1+z$, (c) **3**·3.5MeNO$_2$ with the symmetry operation (*): $0.5+x$, $0.5-y$, $0.5+z$, and (d) **4**·4EtNO$_2$ with the symmetry operation (*): $0.5+x$, $0.5-y$, $0.5+z$, with the selected atom numbering scheme based on the unique atoms (50% probability ellipsoids). Hydrogen atoms are omitted for clarity.

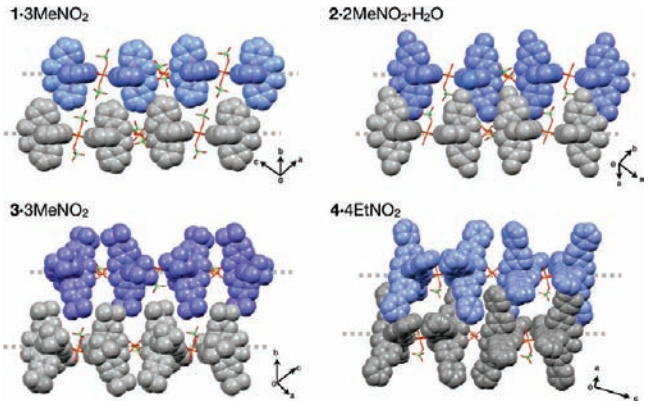

Figure 4. Arrangement of two adjoining chains in four complexes. Ligands are represented by the space filling models.

octahedral coordination sphere with four equatorial carbonyl oxygen atoms ($Fe-O_{carbonyl}$ = 2.057(3)−2.077(3) Å, 2.069(3)−2.082(3) Å, and 2.050(4)−2.100(5) Å for **2**·2MeNO$_2$·H$_2$O, **3**·3.5MeNO$_2$, and **4**·4EtNO$_2$, respectively) and two axial oxygen atoms from a perchlorate ion ($Fe-O_{perchlorate}$ = 2.141(3) and 2.143(3) Å, 2.167(3) Å, and 2.101(13) Å for **2**·2MeNO$_2$·H$_2$O, **3**·3.5MeNO$_2$, and **4**·4EtNO$_2$, respectively) and a water molecule ($Fe-O_{water}$ = 2.117(3) and 2.132(3) Å, 2.086(4) Å, and 2.131(3) Å for **2**·2MeNO$_2$·H$_2$O, **3**·3.5MeNO$_2$, and **4**·4EtNO$_2$, respectively) or two water molecules (2.120(3) and 2.168(3) Å for **4**·4EtNO$_2$). The shortest intrachain $Fe^{II}-Fe^{III}$ distances were estimated to be 5.2155(9) Å, 5.2294(11) Å, and 5.2012(15), respectively. These distances were slightly longer than that in **1**·3MeNO$_2$ by 0.0135 Å to 0.042 Å.

As shown in Figure 4, each chain lies along the $b+c$ vector in **2**·2MeNO$_2$·H$_2$O and along the $a+c$ vector in **3**·3.5MeNO$_2$ and **4**·4EtNO$_2$. The distances between the chains possessing the large substituents (*tert*-butyl or phenyl) were longer, of which the interchain Fe−Fe distances are listed in Table 2. Especially in the case of **4**·4EtNO$_2$, interchain $\pi-\pi$ stacking with C···C distances of ∼3.72 Å and CH−π interaction with C···H distances of ∼3.73 Å were found between the pyridyl moieties and phenyl moieties, respectively (Supporting Information, Figure S3). The interchain interactions and arrangements were not uniform, the disturbance occurred in the $\{Fe^{III}(^{Ph}\mathbf{L})_2\}^+$ units arrangement, and that would cause the disturbance of the equatorial coordination geometry of $\{Fe^{II}(H_2O)_2\}^{2+}$ unit from elongated octahedral geometries. The shortest interchain Fe−Fe distance was estimated to be 11.774(3) Å ($Fe^{II}-Fe^{II}$); however, the chains of **4**·4EtNO$_2$ interacted, meaning that interchain magnetic interactions could be valid for **4**·4EtNO$_2$.

In all complexes, each Fe^{II} ion is surrounded by four carbonyl oxygen atoms in a planar manner, and each Fe^{III}

Table 1. Crystallographic Data for $1\cdot 3MeNO_2$, $2\cdot 2MeNO_2\cdot H_2O$, $3\cdot 3.5MeNO_2$, and $4\cdot 4EtNO_2$

	$1\cdot 3MeNO_2$	$2\cdot 2MeNO_2\cdot H_2O$	$3\cdot 3.5MeNO_2$	$4\cdot 4EtNO_2$
empirical formula	$C_{27}H_{25}Cl_3Fe_2N_9O_{22}$	$C_{30}H_{32}Cl_3Fe_2N_8O_{22}$	$C_{43.5}H_{58.5}Cl_3Fe_2N_{9.5}O_{24}$	$C_{56}H_{55}Cl_3Fe_2N_{10}O_{25.5}$
formula weight	1045.61	1074.69	1316.55	1494.15
temperature/K	200(2)	100(2)	100(2)	100(2)
wavelength/Å	0.71073	0.71073	0.71073	0.71073
crystal system	monoclinic	triclinic	monoclinic	monoclinic
space group	$P2_1/n$	$P\bar{1}$	$P2_1/n$	$P2_1/n$
a/Å	13.701(3)	13.7728(16)	15.207(2)	12.5869(13)
b/Å	18.414(4)	16.1281(19)	21.014(3)	24.806(3)
c/Å	15.352(3)	19.790(2)	19.542(3)	40.164(4)
α/deg		109.849(3)		
β/deg	90.469(9)	91.070(3)	107.860(4)	93.120(3)
γ/deg		90.302(3)		
V/Å^3	3872.9(15)	4133.8(8)	5943.7(14)	12522(2)
Z	4	4	4	8
density (calcd.)/g cm^{-3}	1.793	1.727	1.471	1.585
absorption coeff./mm^{-1}	1.057	0.992	0.708	0.685
F(000)	2116	2188	2724	6144
reflections collected	21541	41980	32236	80535
independent reflections (R(int))	5918 (0.1578)	18980 (0.0997)	12618 (0.0781)	24602 (0.1619)
data/restraints/parameters	5918/0/558	18980/0/1180	12618/0/762	24602/0/1571
goodness-of-fit on F^2	1.043	0.801	0.878	0.847
$R1$ and $wR2$ ($I > 2\sigma(I)$)	0.0851, 0.2307	0.0531, 0.0985	0.0688, 0.1594	0.0842, 0.1894
$R1$ and $wR2$ (all data)	0.1283, 0.2454	0.1192, 0.1075	0.1406, 0.1815	0.2068, 0.2198
largest diff. peak and hole/e Å^{-3}	0.823 and −0.563	1.036 and −0.997	1.055 and −1.111	1.654 and −0.703

Table 2. Selected Atom···Atom Distances (Å)

complex	$1\cdot 3MeNO_2$	$2\cdot 2MeNO_2\cdot H_2O$	$3\cdot 3.5MeNO_2$	$4\cdot 4EtNO_2$
$Fe^{II}-O_{axial}$ (ClO_4)	2.119(6), 2.159(7)	2.141(3), 2.143(3)	2.167(3)	2.101(13)
$Fe^{II}-O_{axial}$ (H_2O)		2.117(3), 2.132(3)	2.086(4)	2.120(6)−2.168(6)
$Fe^{II}-O_{eqatrial}$	2.030(6)−2.077(6)	2.057(3)−2.077(3)	2.069(3)−2.082(3)	2.050(5)−2.100(5)
Fe···Fe (intrachain)	5.1878(19), 5.1954(19)	5.2155(9)−5.2346(9)	5.2294(11), 5.2560(11)	5.2012(15)−5.2522(15)
Fe···Fe (interchain)[a]	10.011(2)	9.5549(11)	10.6864(19)	11.774(3)

[a] Only the shortest one is given.

ion is coordinated by two $bpca^-$ analogues in an orthogonal manner. To estimate the effects of steric repulsion from the adjoining chains, which is induced by the substituents on the pyridyl groups, deviations from the ideal plane of the four oxygen atoms around the Fe^{II} ions, as well as from the ideal orthogonal coordination of the two $bpca^-$ analogues around Fe^{III}, were considered. As shown in Figure 5, the former was estimated from a larger dihedral angle(s), θ_a, between two O_3 coordination planes including three carbonyl oxygen atoms surrounding the Fe^{II} ion(s) (O1/O2/O3* and O2/O3*/O4* for complex **1**, for example), and the latter was estimated from the dihedral angles between the two O−C−N−C−O planes surrounding one Fe^{III} ion bound through imide nitrogen atoms (θ_b). The values are summarized in Table 3. The orthogonality of the two chelating sets (θ_b) is close to the ideal one for all complexes reflecting the rigid *fac*-coordination of the $bpca^-$ analogues, which is essential for the formation of twisted XY systems. On the other hand, the θ_a values clearly indicate that the larger substituent groups cause a greater distortion to the coordination geometries around Fe(II) ion, especially in the case of aromatic phenyl groups in $4\cdot 4EtNO_2$. For $4\cdot 4EtNO_2$, the deviation from ideal O_4 plane was remarkably large, which should weaken the easy-plane anisotropy of the Fe^{II} ions itself. We concluded that the uniaxial anisotropy of $4\cdot 4EtNO_2$ would be reduced, which is disadvantageous in relation to the SCM behavior.

The Fe^{II} ions in these complexes have an elongated octahedral coordination surrounded by four carbonyl oxygen atoms from two $bpca^-$ analogues as equatorial donor atoms. The π-donor character of $O_{carbonyl}$ splits the t_{2g} orbital into e_g and b_{2g} orbitals, and therefore the orbital angular momentum should be quenched as found in $1\cdot 3MeNO_2$.[9] The ground state of the Fe^{II} ions is $^5B_{2g}$ rather than $^5T_{2g}$. This coordination geometry leads to easy-plane anisotropy ($D > 0$), showing that the $S = 2$ spin on Fe^{II} ions is located in the equatorial plane involving the carbonyl oxygen atoms.

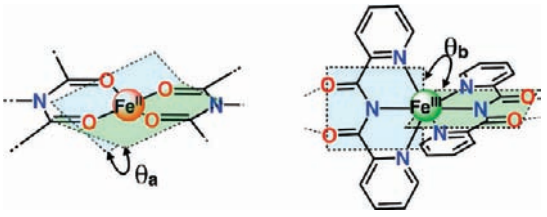

Figure 5. Dihedral angles of two $bpca^-$ analogues around Fe(II) ion (θ_a) and Fe(III) ion (θ_b), which were estimated to evaluate the deviation from the ideal equatorial coordination for the former and from the orthogonal arrangement of the easy-planes for the latter.

Table 3. Dihedral Angles (deg) Used to Evaluate the Coordination Geometry and the Degree of the Divergence of Orthogonal Arrangement of the Easy-Planes

	θ_a (deg)	θ_b (deg)
$1\cdot 3MeNO_2$	0.5(3)	80.4(2)
$2\cdot 2MeNO_2\cdot H_2O$	3.10(15), 3.46(16)	84.97(6), 89.35(6)
$3\cdot 3.5MeNO_2$	3.65(15)	80.26(10)
$4\cdot 4EtNO_2$	17.6(3), 17.9(3)	84.61(19), 84.4(2)

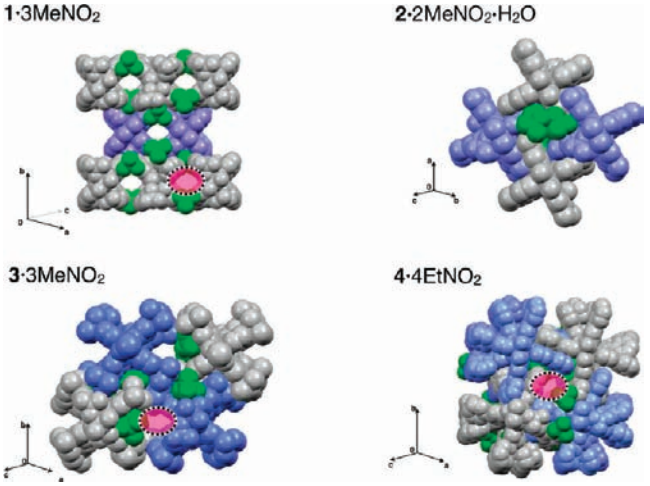

Figure 6. Packing diagram of all compounds viewed from the chain directions. Blue and gray spheres denote cationic chains, green spheres denote perchlorate anions, and pink areas denote the pores.

The cylindrical voids form along the chain axis which are surrounded by four chains in $1\cdot 3MeNO_2$, $2\cdot 2MeNO_2\cdot H_2O$, and $4\cdot 4EtNO_2$, and two chains in $3\cdot 3.5MeNO_2$, as shown in Figure 6. Solvent molecules as well as coordination-free perchlorate anions occupied these voids in a slightly different fashion depending on the complexes. Three nitromethane molecules in $1\cdot 3MeNO_2$ are loosely bound in the pore, and they gradually escape even at room temperature (complete to release for nearly 100 h).[11] In the case of $2\cdot 2MeNO_2\cdot H_2O$, the pores were filled with two coordination-free perchlorate anions, two nitromethane molecules, and a water molecule. The perchlorate anions occupied constricted positions in the voids, which act as spikes, and as a result, the solvent molecules are not easily removed from $2\cdot 2MeNO_2\cdot H_2O$. As described above, $4\cdot 4EtNO_2$ contains many larger solvent molecules which are loosely fixed in the pore showing strong disorder, and loss of them could cause a drastic change in the structure of the chain moiety which will be discussed below.

Structural Changes upon the Loss of Crystalline Solvents. To determine the ease by which the solvent molecules are released, weight loss was measured by using thermo-gravimetric technique for the sample held at a constant temperature of 30 °C under a dry N_2 atmosphere (Supporting Information, Figure S4). The solvent molecules in $2\cdot 2MeNO_2\cdot H_2O$ remain for several hours since the voids are capped by the perchlorate anions. Complexes $3\cdot 3.5MeNO_2$ and $4\cdot 4EtNO_2$ released their solvent molecules similar to $1\cdot 3MeNO_2$.[11] However, the release of molecules was complete in about 30 h, which is much faster than that for $1\cdot 3MeNO_2$ (~100 h), because the voids of these compounds are larger because of the larger substituent groups such as *tert*-butyl and phenyl groups. The weight loss was about 15% for $3\cdot 3.5MeNO_2$ and 18% for $4\cdot 4EtNO_2$, which correspond to the loss of 3.5 $MeNO_2$ molecules for the former (calculated as 16%) and 4 $EtNO_2$ molecules for the latter (calculated as 20%). Elemental analysis also supported the complete loss of solvent molecules and the exchanging with water molecules from the atmosphere (see Supporting Information, Table S4). Since the dried samples should show

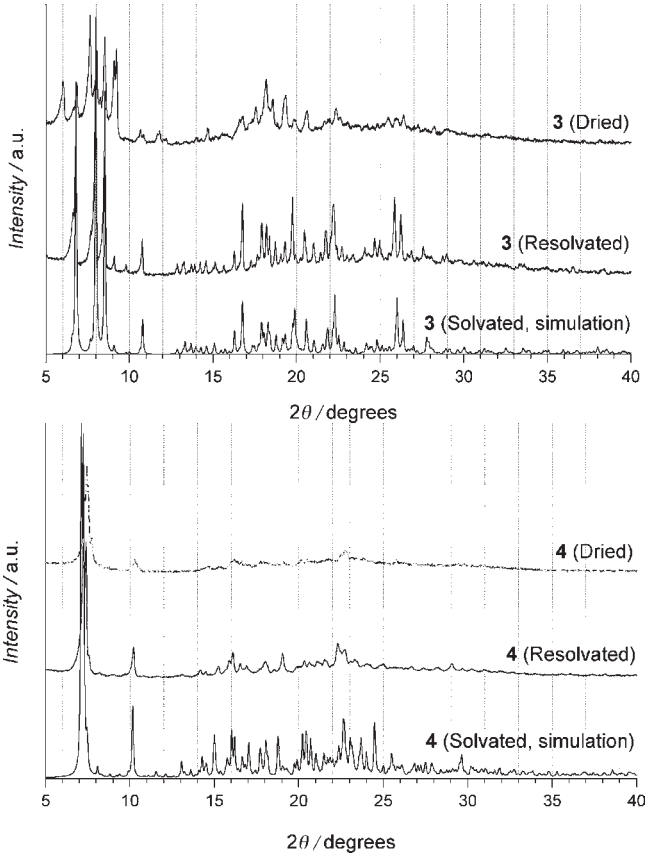

Figure 7. Powder X-ray diffraction pattern measured for dried and resolvated samples of **3** (top) and **4** (bottom) accompanied by simulated patterns based on the single crystal data.

different magnetic behavior from that of the solvated complexes, hereafter, we distinguish between the solvated samples as $1\cdot 3MeNO_2$, $2\cdot 2MeNO_2\cdot H_2O$, $3\cdot 3.5MeNO_2$, and $4\cdot 4EtNO_2$ and dried samples as **1**, **3**, and **4**, respectively.

To confirm the structures of dried samples, X-ray powder diffraction (XRPD) analyses were performed on the powdered samples, which were prepared by crushing the crystals under N_2 and drying for 12 h in the glovebox. In Figure 7, the XRPD patterns of the dried samples were compared with simulated patterns calculated from the single crystal diffraction data of the solvated samples. Complexes **1**[11] and **3** were still crystalline after complete drying, and their XRPD patterns were different from $1\cdot 3MeNO_2$ and $3\cdot 3.5MeNO_2$ (Supporting Information, Table S4). We have reported that the space group of $1\cdot 3.5MeNO_2$ changes from $P2_1/n$ to $C2/c$ when half of $MeNO_2$ molecules are removed by drying.[11] A similar change in the crystal system and/or space group occurred upon drying to produce complex **3**. After an exposure of **3** in the vapor of $MeNO_2$, the complex was solvated again to give a sharp XRPD pattern which is very similar to that of the simulated one for the single crystal of $3\cdot 3MeNO_2$; however, the reversibility is not complete, and after the second drying process, the pattern lost some signals which were observed after the first drying process (Supporting Information, Figure S5). No XRPD pattern was observed in the high θ range for complex **4**, implying that it became amorphous. The amorphous character was maintained after an exposure

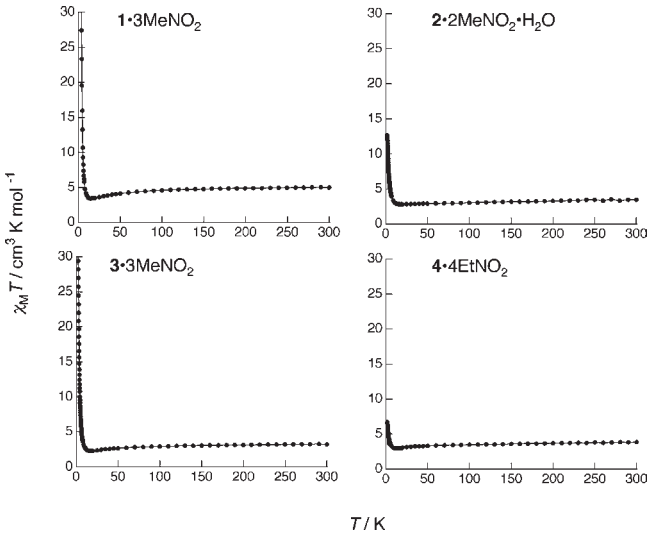

Figure 8. Temperature dependence of $\chi_M T$ for $\mathbf{1}\cdot 3MeNO_2$ (top left), $\mathbf{2}\cdot 2MeNO_2\cdot H_2O$ (top right), $\mathbf{3}\cdot 3.5MeNO_2$ (bottom left), and $\mathbf{4}\cdot 4EtNO_2$ (bottom right) measured under the magnetic field of 100 Oe. The solid lines are guides for the eyes.

of **4** in the vapor of $EtNO_2$. In other words, the solvent molecules in the voids of $\mathbf{4}\cdot 4EtNO_2$ highly stabilize the crystal structure.

Magnetic Properties. DC magnetic measurements were performed on polycrystalline samples between 300−1.8 K in magnetic field of 100 Oe (Figure 8). $\mathbf{2}\cdot 2MeNO_2\cdot H_2O$, $\mathbf{3}\cdot 3.5MeNO_2$, and $\mathbf{4}\cdot 4EtNO_2$ showed temperature dependences of the $\chi_M T$ values similar to that of $\mathbf{1}\cdot 3MeNO_2$. The $\chi_M T$ values of each compound decreased upon lowering the temperature, suggesting the presence of antiferromagnetic interactions between adjoining metal ions through the $bpca^-$ derivative ligands.

The $\chi_M T$ values for $\mathbf{2}\cdot 2MeNO_2\cdot H_2O$ decreased from 3.46 cm^3 K mol^{-1}, which is slightly larger than the expected spin only value of 3.37 cm^3 K mol^{-1} for one Fe^{II} ion ($S = 2$, high-spin) and one Fe^{III} ion ($S = 1/2$, low-spin) with an average g value of 2, upon lowering the temperature to 20 K. On lowering the temperature, the $\chi_M T$ values increased abruptly, reaching a maximum value of 12.67 cm^3 K mol^{-1} at 1.8 K. This temperature dependence of the $\chi_M T$ values for $\mathbf{2}\cdot 2MeNO_2\cdot H_2O$ is clearly consistent with the presence of a ferrimagnetic arrangement of adjoining spins.

The $\chi_M T$ values for $\mathbf{3}\cdot 3.5MeNO_2$ decreased from 3.98 cm^3 K mol^{-1} (300 K), which is again slightly larger than the expected spin only value given above, upon lowering the temperature down to 20 K. Below 20 K, the $\chi_M T$ values increased abruptly, reaching a maximum value of 29.57 cm^3 K mol^{-1} at 1.8 K.

The $\chi_M T$ values for $\mathbf{4}\cdot 4EtNO_2$ decrease from 3.08 cm^3 K mol^{-1} at room temperature to give the minimum value at 12 K. Then the $\chi_M T$ values increased leaching to a maximum value of 6.39 cm^3 K mol^{-1} at 1.8 K. The maximum value of $\chi_M T$ is roughly related to the correlation length of the SCM at that temperature, and the smallest value observed for $\mathbf{4}\cdot 4EtNO_2$ implies that the magnetic correlation length of this complex is shorter than others.

The character and the degree of magnetic anisotropy of the Fe^{II} ion could be estimated from the $\chi_M T - T$ curves,

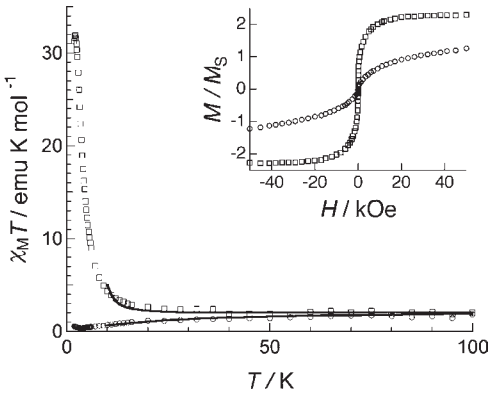

Figure 9. Magnetic measurements on oriented single crystals of $\mathbf{3}\cdot 3.5MeNO_2$ with the field applied along the chains (squares) and perpendicular to the chains (circles). Temperature dependence of the $\chi_M T$ at below 100 K with the theoretical lines corresponding to the best fits obtained with the spin Hamiltonian (see text). Inset: Field dependence of the magnetization at 1.8 K.

which were measured for single crystal(s) in a magnetic field applied parallel and perpendicular to the chain axis. Since only single crystals of $\mathbf{3}\cdot 3.5MeNO_2$ were large enough to perform this experiment, the exchange interaction between adjoining $Fe^{II}-Fe^{III}$ ions (J) and the single ion magnetic anisotropy of Fe^{II} (D) were estimated only for single crystals of $\mathbf{3}\cdot 3.5MeNO_2$. Needle-like single crystals were oriented in one direction, and the magnetic susceptibility data were collected with the field applied along the needles and from the side of the needles, which are parallel (crystallographic $a+c$ vector) and perpendicular to the chain, respectively (Figure 9). The anisotropy of the susceptibility was observed below 40 K. When the field was applied along chain, the $\chi_M T$ values abruptly increased on lowering the temperature, which suggests the presence of an easy-axis in this direction. The anisotropy was also confirmed by the field dependence of magnetization (at 1.8 K, see inset of Figure 9), which quickly saturated when the field was applied along the chain; however, no saturation was found when the field was applied perpendicular to the chain. The temperature dependence of $\chi_M T$ was analyzed using the following spin Hamiltonian:

$$H = -2J\sum_i [S_{4i}\cdot S_{4i+1} + S_{4i+1}\cdot S_{4i+2} + S_{4i+2}\cdot S_{4i+3} + S_{4i+3}\cdot S_{4i+4}] + D\sum_i [(S^x_{4i})^2 + (S^y_{4i+2})^2] + H_{Zeeman} \quad (1)$$

where S_j is either an $S = 2$ spin for Fe^{II} for even values of j or an $S = 1/2$ spin for Fe^{III} for odd values of j, J is the superexchange interaction between neighboring Fe^{II} and Fe^{III} ions in the chain, and D is the uniaxial zero-field splitting parameter for Fe^{II} spins. The chain is lying along z-axis, and magnetic easy-planes are parallel to the zx-plane for the spins of $j = 4i$ (S^x_{4i}) or the yz-plane for the spins of $j = 4i+2$ (S^y_{4i+2}). Using a mean-field approximation of the Hamiltonian, the parameters J/k_B and D/k_B were estimated to be −6 and +18 K, respectively. We have reported that the J/k_B and D/k_B values for $\mathbf{1}\cdot nMeNO_2$ ($3 > n$) are approximately −9 and +24 K, respectively, using the same Hamiltonian.[9a] The overall easy-axial

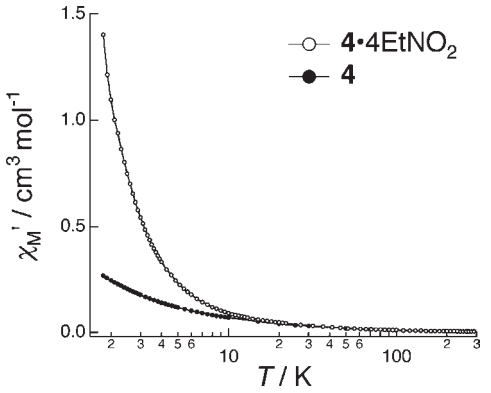

Figure 10. Temperature dependences of χ_M' of **4**·4EtNO$_2$ (open circles) and **4** (filled circles) under zero-field. The solid lines are guides for the eyes.

anisotropy of the chain arises from the twisted arrangement of easy-plane of the Fe^{II} ions along the chain.

In the crystal structure of **4**·4EtNO$_2$, close $C_{phenyl}-C_{phenyl}$ and C−H contacts were found, indicating the presence of interchain magnetic interactions through $\pi-\pi$ and CH$-\pi$ stacking. However, on the bases of the χ_M' versus T plots (Figure 10), interchain interactions associated with the Curie or Néel point, which implies the presence of long-range ordering, were not found above 1.8 K. Therefore, interchain interactions through the overlapping of the phenyl groups are negligible in this temperature range.

AC magnetic measurements were performed on randomly oriented microcrystalline samples of **2**·2MeNO$_2$·H$_2$O and **4**·4EtNO$_2$ in the temperature range 1.8−3.5 K and randomly oriented microcrystalline sample of **3**·3.5MeNO$_2$ in the range 1.8−4.0 K, respectively. Figure 11 shows the ac susceptibility features of all compounds measured at various ac frequencies (5−997 Hz). Below 3.5 K, the ac susceptibilities, χ_M' and χ_M'', which are the in-phase and out-of-phase components, showed strong frequency dependences for each compound, which rules out a three-dimensional transition and suggests a presence of a thermally activated relaxation process. When the temperature was lowered, the χ_M' signal increased to a maximum value and then decreased accompanied by the appearance of the χ_M'' signal, which was attributed to a blocking process of magnetization. When the thermal energy is not sufficient for the reverse of the magnetization, the peak tops of the χ_M'' signal appear at each frequency at different temperatures. Below the temperature for the appearance of the peak tops, the motion of the entire magnetization becomes frozen, and this temperature is defined as the blocking temperature (T_B). The ac response disappears at temperatures less than T_B. **2**·2MeNO$_2$·H$_2$O and **3**·3.5MeNO$_2$ have a value of T_B similar to **1**·3MeNO$_2$ (T_B at 997 Hz: 2.3 K for **1**·3MeNO$_2$, 2.3 K for **2**·2MeNO$_2$·H$_2$O, 2.8 K for **3**·3.5MeNO$_2$), whereas **4**·4EtNO$_2$ has lower T_B (2.0 K at 997 Hz) compared to that of **1**·3MeNO$_2$. This implies that a structural perturbation changes the SCM behavior in this twisted arrangement of easy-plane system. Nearly semicircle Cole−Cole diagrams (χ_M'' versus χ_M', Figure 12) were obtained for all compounds at fixed temperatures, and they were analyzed by using a generalized Debye model, wherein the α parameter quantifies the width of the relaxation

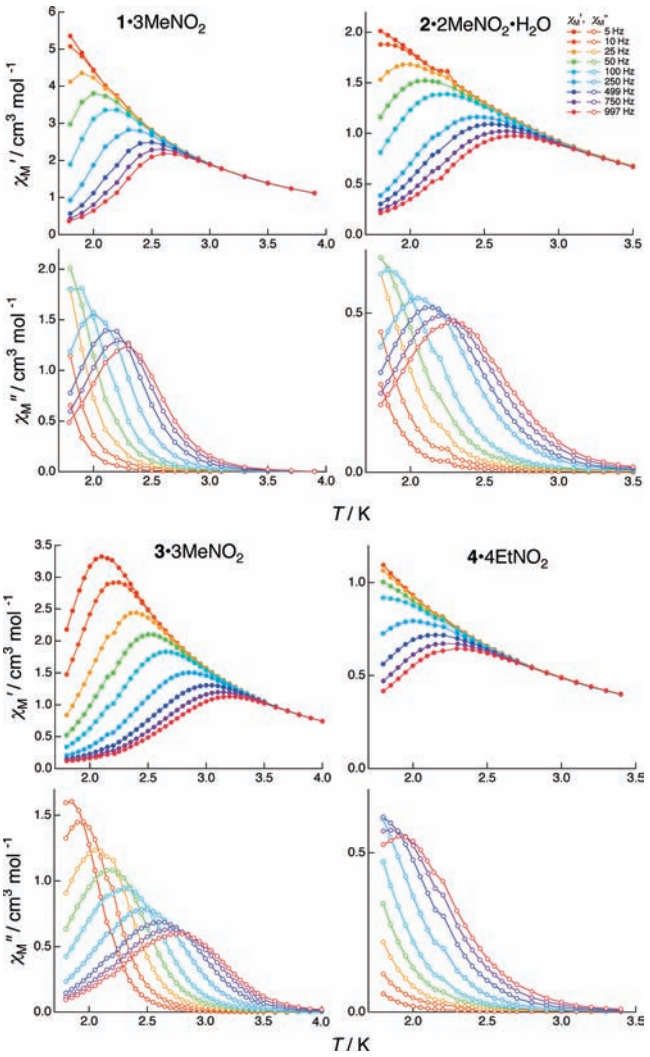

Figure 11. Temperature dependence of the real χ_M' (filled circles) and imaginary χ_M'' (open circles) components of the ac susceptibility measured in zero applied field. The solid lines are guides for the eyes.

time (τ) distributions.[17] Indeed, the experimental data of all compounds were well reproduced with small α values: 0.22(5)−0.25(2) for **2**·2MeNO$_2$·H$_2$O, 0.13(2)−0.19(2) for **3**·3.5MeNO$_2$, and 0.27(2)−0.28(5) for **4**·4EtNO$_2$. The small α values indicate that the relaxation occurred via a single relaxation process, and thus, the relaxation time can be obtained from the Arrhénius equation:

$$\tau = \tau_0 \exp(\Delta/k_B T_B), \quad \tau = (2\pi\nu_{ac})^{-1}$$

where τ_0 is a pre-exponential factor characteristic of the system, Δ is the activation energy barrier, and k_B is the Boltzmann constant. From Arrhénius plots (Figure 13), the values of τ_0 and Δ/k_B were estimated for **2**·2MeNO$_2$·H$_2$O and **3**·3.5MeNO$_2$, which are summarized in Table 4. Since only a few χ_M'' peak tops were observed above 1.8 K for **4**·4EtNO$_2$, the analysis could not be performed for this complex.

Compounds **2**·2MeNO$_2$·H$_2$O and **3**·3.5MeNO$_2$ showed typical SCM character above 1.8 K, which is similar to

(17) (a) Aubin, S. M. J.; Sun, Z.; Pardi, L.; Krzystek, J.; Folting, K.; Brunel, L.-C.; Rheingold, A. L.; Christou, G.; Hendrickson, D. N. *Inorg. Chem.* **1999**, *38*, 5329. (b) Cole, K.; Cole, R. H. *J. Chem. Phys.* **1941**, *9*, 341.

$1 \cdot 3MeNO_2$. In the case of $4 \cdot 4EtNO_2$, although we could not quantitatively analyze the Arrhénius plot, the relaxation process of magnetization in $4 \cdot 4EtNO_2$ occurs via a single relaxation process similar to the other compounds. Therefore, if the twisting arrangement of easy-planes of Fe^{II} ions is retained upon the introduction of various substituents on $bpca^-$, each compound should have SCM character similar to that of $1 \cdot 3MeNO_2$. $1 \cdot 3MeNO_2$, $2 \cdot 2MeNO_2 \cdot H_2O$, and $3 \cdot 3.5MeNO_2$ showed very similar magnetic properties down to 1.8 K, and the effects of the substituents on the interchain interactions were rather small for them.

To investigate a presence or an absence of interchain magnetic interactions, we determined the magnetic behaviors of $1 \cdot 3MeNO_2$ and $3 \cdot 3.5MeNO_2$ in a lower temperature range down to 0.5 K. In $1 \cdot 3MeNO_2$, an interchain antiferromagnetic interaction appeared at 1.0 K, which was observed as a sigmoid curve in the magnetization process correlated with the metamagnetic behavior (Figure 14). At 0.5 K, a hysteresis curve characteristic of a three-dimensional bulk magnet with a coercive force, H_c, of 300 Oe was obtained. These were backed by the data of heat capacity measurements on single crystals, which showed a typical λ-type shape around 1.0 K, indicating the presence of long-range ordering at this temperature (Supporting Information, Figure S6). $1 \cdot 3MeNO_2$ underwent a phase transition from isolated SCM to a bulk magnet, which interacts with the surrounding chains.

On the other hand, the absence of long-range ordering in $3 \cdot 3.5MeNO_2$ was confirmed from the magnetization curve, which did not have a sigmoid shape down to 0.5 K, because of a wider interchain separation caused by the steric *tert*-butyl groups (Supporting Information, Figure S7). $3 \cdot 3.5MeNO_2$ maintained SCM character down to 0.5 K, and the results show that bulky substituents can be used to control the interchain magnetic interactions.

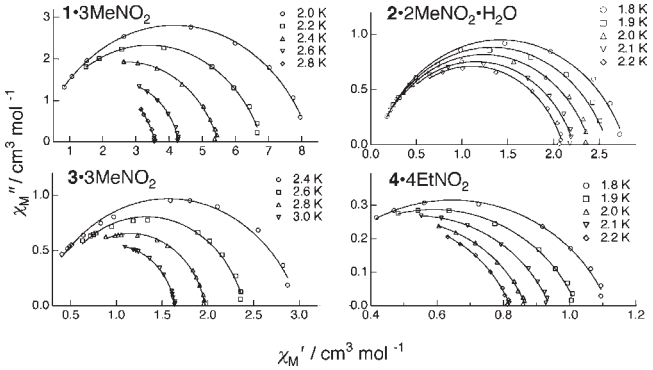

Figure 12. Cole−Cole diagrams at the fixed temperature. The solid lines represent the least-squares fit obtained with an extended Debye model (see text).

Solvent Induced Change of Magnetic Properties. To investigate the effects of the absorption/desorption of the crystalline solvent molecules on the magnetic properties, the temperature dependence of the magnetic susceptibilities data of freshly prepared solvated samples ($1 \cdot 3MeNO_2$, $3 \cdot 3.5MeNO_2$, and $4 \cdot 4EtNO_2$) and completely dried samples (**1**, **3**, and **4**), which were prepared by the keeping of the crystalline solvated complexes under a dry nitrogen atmosphere, were investigated (Figure 15). Complex $2 \cdot 2MeNO_2$ retained its crystalline solvents under the drying conditions, and thus, the temperature dependence of magnetic susceptibilities did not change (Supporting Information, Figure S8).

The $\chi_M T$ values of solvated and dried samples at room temperature were almost similar to each other (4.49, 3.98, and 3.08 $cm^3\ K\ mol^{-1}$ for $1 \cdot 3MeNO_2$, $3 \cdot 3.5MeNO_2$, and $4 \cdot 4\ EtNO_2$, and 4.39, 3.64, and 3.15 $cm^3\ K\ mol^{-1}$ for **1**, **3**, and **4**, respectively). Below 20 K, both **1** and **3**, which maintained their crystallinity under the drying conditions, showed similar temperature dependences of $\chi_M T$. The dependences were typical of a ferrimagnetic arrangement of the spins of neighboring Fe^{II} and Fe^{III} ions. $1 \cdot 3MeNO_2$ and $3 \cdot 3.5MeNO_2$ did not show a peak top down to 1.8 K, whereas both **1** and **3** showed a peak top. $4 \cdot 4EtNO_2$ showed a different trend because of the loss of crystalline solvents. As mentioned above, the $\chi_M T$ values of solvated $4 \cdot 4EtNO_2$ gradually increased with a decrease in the temperature; however, no peak was observed down to 1.8 K. On the other hand, the $\chi_M T$ values of **4** monotonically decreased down to 1.8 K, indicating that there is no ferrimagnetic spin arrangement of the adjoining Fe^{II} ions via Fe^{III} ion. The interchain magnetic interactions were investigated on the basis of the χ_M' versus T plot

Table 4. Magnetic Parameters Obtained for $1 \cdot 3MeNO_2$, $2 \cdot 2MeNO_2 \cdot H_2O$, $3 \cdot 3.5MeNO_2$, and $4 \cdot 4EtNO_2$

compounds	Δ/k_B (K)	τ_0 (s)	α at 2.4 K	J/k_B (K)	D/k_B (K)
$1 \cdot 3MeNO_2$	22.5(4)	7.6×10^{-9}	0.21(3)	−8.4(5)	+24.1(5)
$2 \cdot 2MeNO_2 \cdot H_2O$	21.8(18)	1.1×10^{-8}	0.22(5)		
$3 \cdot 3.5MeNO_2$	28.8(3)	5.6×10^{-9}	0.13(17)	−5.7(2)	+17.7(2)
$4 \cdot 4EtNO_2$			0.27(2)		

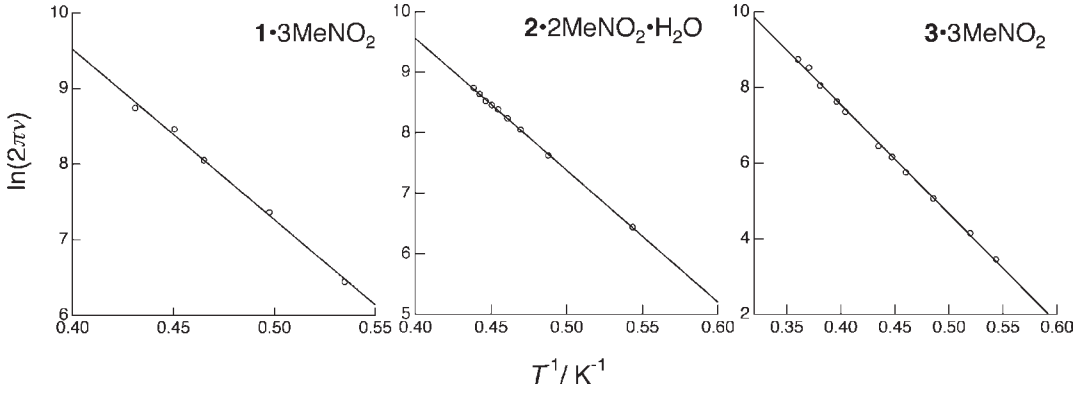

Figure 13. Arrhénius plots. The solid lines represent the least-squares fits of the experimental data to the Arrhénius equation (see text).

(Figure 10). The monotonic increase of χ_M' on lowering the temperature clearly indicates that the interactions were negligibly small in **4** in this temperature range.

The frequency dependences of ac susceptibilities of **1**, **3**, and **4** were measured under conditions similar to those for the solvated samples (in-phase components: Supporting Information, Figure S9, out-of-phase components: Figure 16). Below 4.0 K, the χ_M' and χ_M'' values of **1** and **3** showed strong frequency dependencies being typical of SCMs, whereas **4** did not show any out-of-phase signals, which is consistent with the dc studies shown above. **4** lost the SCM character during the drying process, indicating that a transition between a superparamagnetic phase and a paramagnetic phase occurred.

Semicircle Cole−Cole diagrams of **1** and **3** were obtained with small α values of 0.14(2) and 0.06(2), respectively, from which we concluded that the spin relaxation occurs via single relaxation process (Supporting Information, Figure S10). Therefore, complexes **1** and **3** maintain the SCM character in both the solvated and the dried states. The values of T_B were 0.6 K higher for **1** and 1.0 K higher for **3** than those of the solvated complexes in a 997 Hz ac field. For **1**·3MeNO$_2$ and **3**·3.5MeNO$_2$, the Arrhénius plots could be analyzed with single lines to give Δ/k_B values of 22.5(4) K and 28.8(3) K, respectively. For **1** and **3**, finite-size effects were observed, and their Arrhénius plots had to be fitted with two lines (Figure 17).[2,5,18] The obtained slopes, Δ_1/k_B and Δ_2/k_B, for the higher and the lower temperature ranges, were estimated to be 37.4(4) K and 24.9(2) K for **1** and 53(2) K and 32(2) K for **3**, respectively. Although detailed theoretical analyses of the spin relaxation process were impossible because of the complexity of structures and the spin states because of the ferrimagnetic character, some information could be obtained from a plot of $\ln(\chi_M'T)$ versus T^{-1} (χ_M': in-phase components of the ac susceptibility at 1 Hz), including the exchange energy (J) of an Ising chain system[18] (Supporting Information, Figure S11). It is known that the $\chi_M'T$ value for a ferromagnetic Ising chain shows exponential behavior defined as $\chi_M'T = C\exp(\Delta_\xi/T)$, where C, ξ, and Δ_ξ denote the Curie constant, magnetically correlated length, and correlation energy, respectively. For the ideal system, a plot of logarithm of $\chi_M'T$ versus T^{-1} should afford a straight line, and Δ_ξ, which is correlated to the magnetic interaction J, can be estimated from the slope. Although our complexes are not exactly the case of a ferromagnetic Ising system, such linearity was found in the temperature range below 15 K, and the correlation energy could be estimated. The values of Δ_ξ/k_B of **1** and **3** (15.5(2) and 14.59(9) K) were two or three times larger than those of **1**·3MeNO$_2$, **3**·3.5MeNO$_2$ (5.16(4) and 7.27(2) K). In general, the SCM character could be described as a function of the magnetic anisotropy parameter D, the exchange interaction J, and the spin degeneracy S. The increase of Δ_ξ values indicate that the enhancement in the SCM behaviors of complexes **1** and **3** during the drying process is mainly due to the increase in the J values, which would result in the shrinking of the cell by release of the crystalline solvent molecules. The conversion of the magnetism between those of solvated **1**·3MeNO$_2$ and dried **1** has been reported previously. This complex showed a reversible change between an enhancement and a weakening of SCM features after the drying and the resolvating processes. However, change in magnetism for **3**·3.5MeNO$_2$ was irreversible (Figure 18) being related to the structural irreversibility described above. Although complex **3** behaves as an SCM after drying/resolvating processes, the enhancement of SCM behavior was not observed after the second drying process.

The magnetism of **4**·4EtNO$_2$ showed a drastic change from SCM to non-SCM upon the loss of crystallizing solvent, accompanied with a drastic change from crystals to an amorphous state, whereas such a dramatic change was not observed in the cases of **1** and **3**. This may be related to how the solvent molecules occupy the void

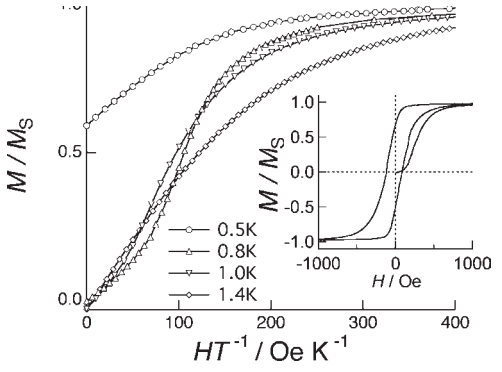

Figure 14. Field dependences of the magnetization measured on single crystals of **1**·3MeNO$_2$ to the easy magnetization directions (chain axis) at the different temperatures. Inset: The hysteresis curve of magnetization at 0.5 K. The solid lines are guides for the eyes.

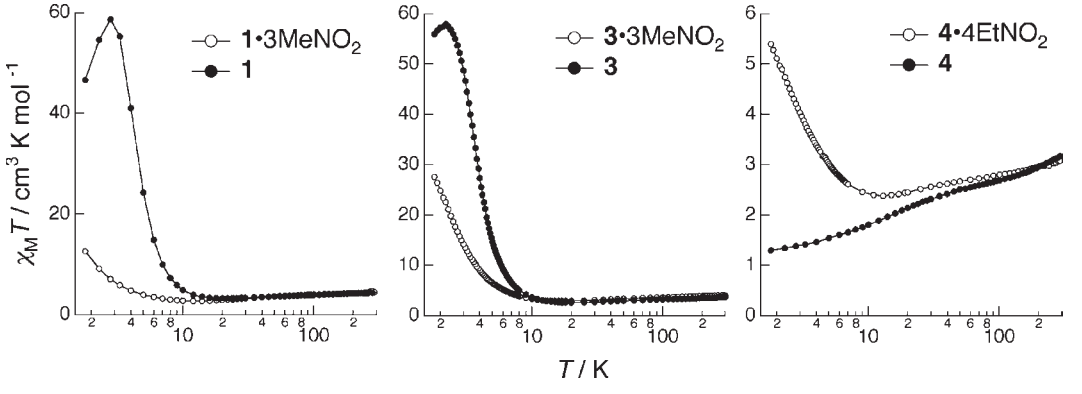

Figure 15. Temperature dependence of $\chi_M T$ for the solvated and dried condition samples (under 100 Oe). The solid lines are guides for the eyes.

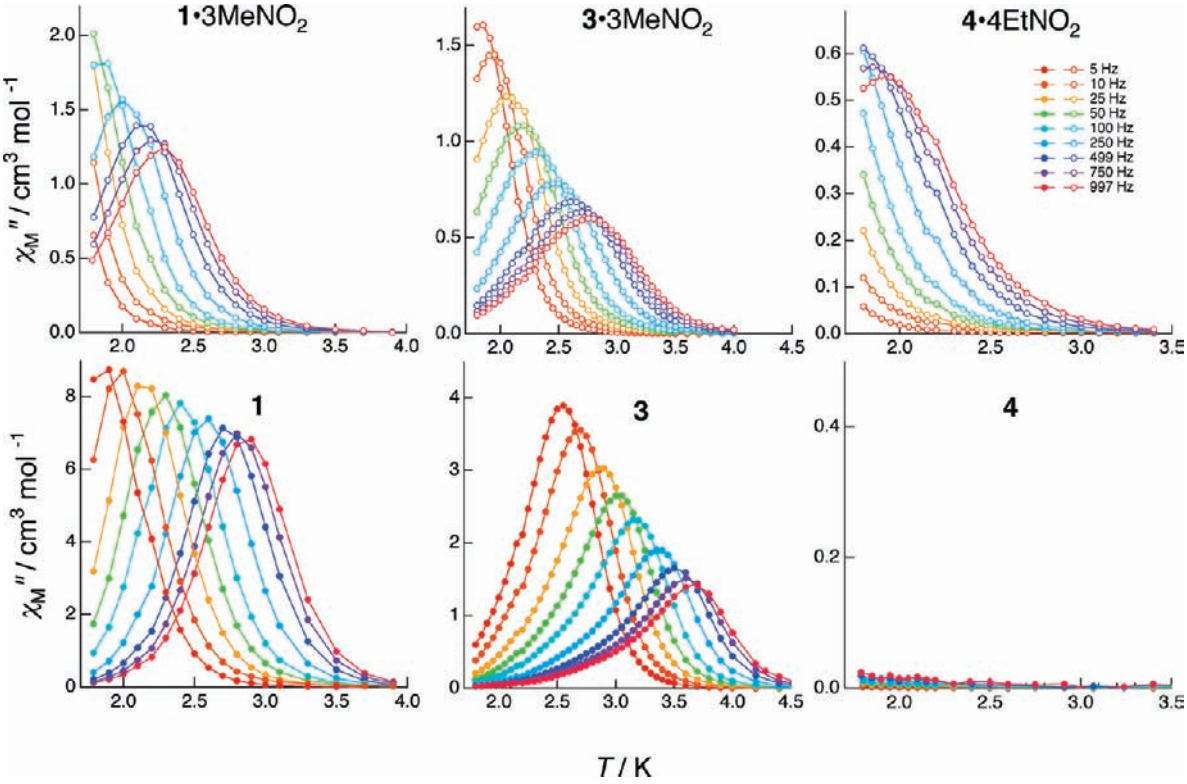

Figure 16. Imaginary components of the ac susceptibilities of the solvated condition samples (open circles) and the dried condition samples (filled circles) in a 3 Oe oscillating at the different frequencies (5−997 Hz). Solid lines are guides for the eyes.

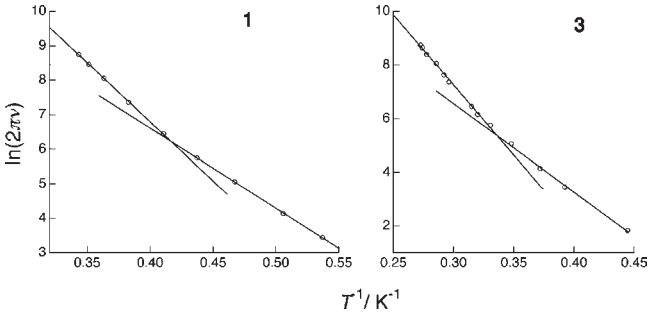

Figure 17. Arrhénius plots for **1** and **3**. The solid lines represent the least-squares fits of the experimental data to the Arrhénius equation (see text).

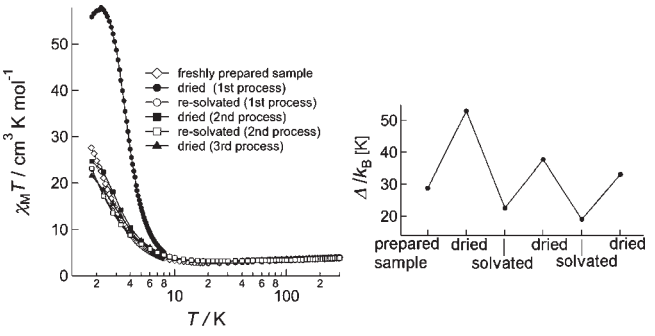

Figure 18. Temperature dependence of $\chi_M T$ (left) and estimated Δ/k_B values (right) of complex **3** measured after some drying/resolvating processes.

space around the chain frameworks. The void space in the single crystals became larger as the substituted groups became more bulky, and the number of the occupying molecules and ions increased as well: one ClO_4^- and three $MeNO_2$ in **1**, two ClO_4^- and 3.5 $MeNO_2$ in **3**, and 2.5 ClO_4^- and four $EtNO_2$ in **4**. In **1**·3$MeNO_2$ and **3**·3.5$MeNO_2$, the crystalline solvents occupied only the voids spaces formed among the chain frameworks, whereas, in **4**·4$EtNO_2$, they occupied the void spaces among and inside the frameworks, which might stabilize the bulky structure of **4**·4$EtNO_2$. In other words, the solvents in **4**·4$EtNO_2$ may contribute to the stabilization of the chain structure more than those in **1**·3$MeNO_2$ and **3**·3.5$MeNO_2$, and thus, a dramatic change was induced in **4** with the removal of the crystallizing solvents. In the twisted XY system, the easy-axis of the SCM arises from the strict orthogonal arrangement of the easy-planes of the Fe^{II} ions along the chain, and hence, a deviation from the ideal arrangement of the easy-planes will cause a reduction in the uniaxial anisotropy, which leads to the loss of the SCM character. Removal of the crystalline solvents in compound **4**·4$EtNO_2$ could reduce the regularity in orthogonal arrangement of easy-planes, resulting in the complete loss of SCM character. Compound **4**·4$EtNO_2$ underwent a transition between superparamagnetic and paramagnetic states accompanied by a transition from a crystal state to an amorphous state.

Conclusion

In this study, we synthesized a family of SCMs, of which the SCM character originated from the spatial arrangement of high spin Fe^{II} ions with easy-plane anisotropy. Since the

(18) Coulon, C.; Miyasaka, H.; Clerac, R. *Struct. Bonding* (*Berlin*) **2006**, *122*, 163.

magnetic anisotropy of the entire chain is strongly correlated to the orthogonal alignment of the easy-planes as well as the magnetic interaction between adjoining Fe(II) ions, the magnetic behaviors of these complexes were very sensitive to the subtle structural changes, which occurred because of the introduction of peripheral substitutents as well as the loss of the crystalline solvent molecules. Although we have introduced three different substituent groups with different bulkiness, it had little effect on the core structures of Fe(II)−Fe(III) alternate chains, and the resulting complexes maintain an SCM feature similar with the original complex. Freshly prepared complexes **1**·3$MeNO_2$, **2**·2$MeNO_2$·H_2O, and **3**·3.5$MeNO_2$ showed SCM features which is confirmed from dc and ac susceptibility measurements, exhibiting a ferrimagnetic character with an antiferromagnetic interaction between adjusting Fe(II) and Fe(III) ions with similar magnitude, and exhibiting a slow magnetic relaxation at around 2.5 K with the similar barrier for spin flipping with the height of 22−29 K. It seems that the presence/absence of a substitution group at the 4-position of the pyridine ring does not affect the magnetic behavior from the viewpoint of electron withdrawing/donating characters. In the case of **4**, a slightly disordered array of the equatorial plane from the regular orthogonal arrangement was achieved by the introduction of bulky phenyl groups, and this resulted in a weakening of the SCM character of **4**. We assume that the weakening of the SCM feature would be due to the structural factors more than the electronic factors, since the Hammett parameter σ_p of phenyl group is very close to that of H. The introduction of substitutents on the $bpca^-$ ligand is a good way to control the interchain magnetic behavior, which affects the long-range magnetic ordering driven by the very weak interchain interactions down to 0.5 K.

Solvent induced changes in the magnetic properties were also investigated. Both the solvated and dried forms of **1** and **3** showed characteristics of a SCM, and the energy barrier Δ/k_B increased with the loss of the crystalline solvents. The correlation energies of the Ising spins, Δ_ξ, increased as determined from the semilog plots of $\chi_M'T$ versus T^{-1}. These values are related to the exchange energies, J, and therefore, the removal of the crystallizing solvents enhances magnetic interactions among the Fe ions, which causes a transition between two different superparamagnetic states. In the case of **4**·4$EtNO_2$, a transition between superparamagnetic and paramagnetic states was observed. **4** lost its SCM character upon the loss of the crystalline solvents, which reduced the regularity of the orthogonal arrangement of easy-planes and caused it to become amorphous.

To the best of our knowledge, this is the first observation of a transition between two superparamagnetic states or between a superparamagnetic state and a paramagnetic state for SCMs. This phenomenon appears to be the structural flexibility and the sensitivity of magnetic properties of the twisted XY systems.

Acknowledgment. We thank Prof. H. Miyasaka, Tohoku University, for useful discussion of the magnetism. This work was supported by a Grant-in Aid for Scientific Research (C) from the Ministry of Education, Culture, Science, Sports, and Technology, Japan.

Supporting Information Available: Crystallographic details in CIF format, crystal data for **9** and **12** (Tables S1 and S2), Ortep drawings of **9** and **12** (Figures S1 and S2), elemental analyses (Table S3), stacking diagram of **4**·4$EtNO_2$ (Figure S3), plots of weight loss for **2**·2$MeNO_2$·H_2O, **3**·3.5$MeNO_2$, and **4**·4$EtNO_2$ (Figure S), PXRD pattern measured for solvated and dried sample of **3** (Figure S5), temperature dependence of **1**·3$MeNO_2$ (Figure S6), field dependence of magnetization of **3**·3.5$MeNO_2$ at low temperature (Figure S7), dc and ac susceptibility data of **2**·2$MeNO_2$·H_2O (Figure S8), ac data of solvated and dried sample of **1**, **3**, and **4** (Figure S9), Cole−Cole diagram of **1** and **3** (Figure S10), $\ln(\chi'T)$ versus T^{-1} plot of solvated and dried sample of **1** and **3** (Figures S11). This material is available free of charge via the Internet at http://pubs.acs.org.